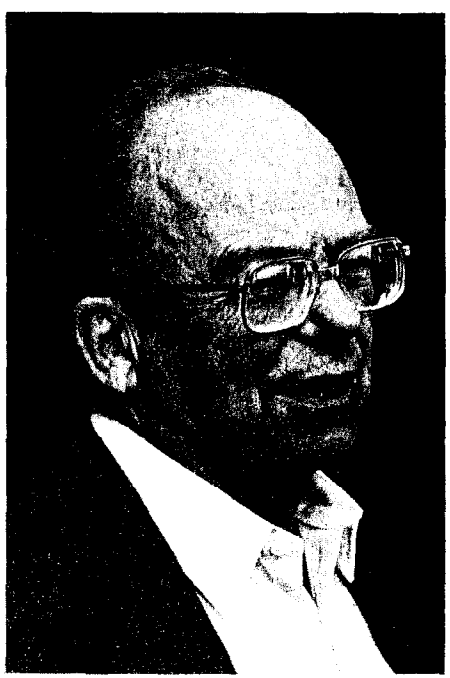

INCLUSIVE LEPTON-HADRON EXPERIMENTS

J. Steinberger

CERN, Geneva, Switzerland

1. INTRODUCTION

We are here today to honor Pief because we are his friends, we recognize and admire his contributions to physics and to society and we want to express this. Among these achievements is the creation of the SLAC Laboratory. Under the direction of Pief, SLAC has become a great laboratory, a focus and center for particle physics and physicists. And SLAC can congratulate itself on two fundamental discoveries, one of which is the cornerstone of the topic I have been assigned. These successes are not only to the credit of the experimenters responsible, but also in large measure to the credit of Pief, as father of the laboratory, as director, as guru, and as a participant, and the organizers of the Pief-Fest were right in putting these experiments on the program. If I was asked to recall one of them, I do not think it is because I am a great expert on the subject. I rather imagine it is because in our early days Pief and I had the pleasure of working together, in the days when interesting physics could be done in a few weeks by one or two people, and I am glad that the organizers remembered also these early days of Pief. I have been asked to talk about lepton scattering. In order to make a reasonably cohesive story I have picked out two topics: the inclusive scattering experiments which are responsible for our understanding of nucleon structure, and the neutral current experiments which were crucial in the history of the electroweak interaction. But it is necessary at least to mention two earlier fundamental discoveries of lepton scattering experiments: the electron scattering experiments performed here at Stanford by Hofstadter and colleagues and which found the nuclear form factors,[1] and the first high-energy neutrino experiment, the Columbia-BNL experiment[2] which showed that the muon and electron neutrinos are distinct.

Many of you know the topics that it is my privilege to recall here more thoroughly than I do. Nevertheless, I hope that it will give you a certain amount of pleasure to see again some of the results which contributed so much to the spectacular advance in our understanding of particles which characterizes these past dozen years.

2. NUCLEON STRUCTURE AND THE STRONG INTERACTION

2.1 Prehistory

Among the earliest inelastic lepton-hadron experiments were those of Panofsky and others on electroproduction of pions[3-6] at the Stanford HEPL 600 MeV linear accelerator in the mid 1950s. In the light of subsequent developments, one of the more interesting results was the realization, in the last of the quoted papers, that it is of greater interest to detect the final-state electron than the produced pion, the method followed previously. Figure 1 shows

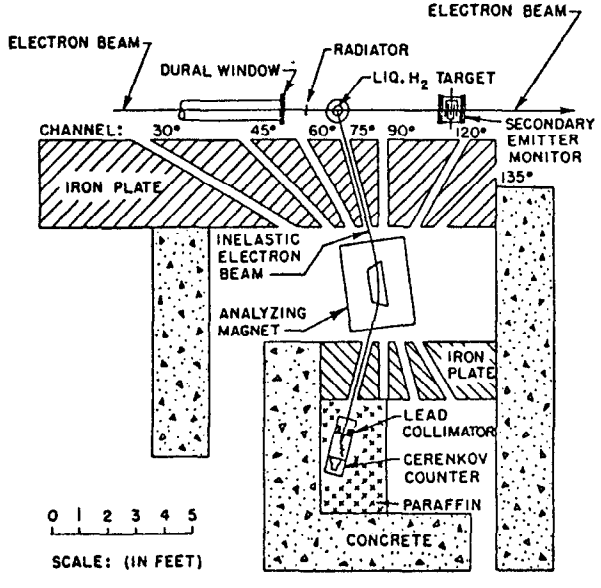

Fig. 1 Apparatus for the measurement of the electroproduction of pions in which the scattered lepton is detected rather than the pion. (Ref. 6.)

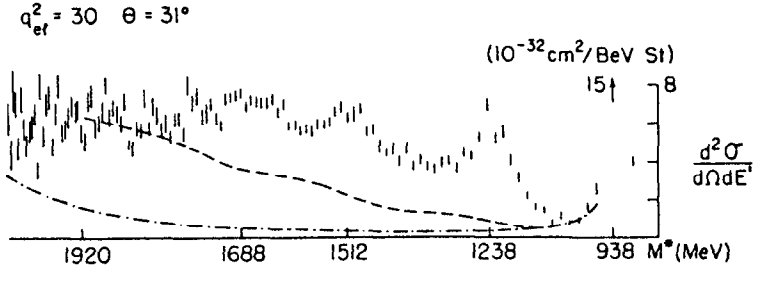

Fig. 2 Baryon resonance excitation in inclusive electron scattering at CEA. (Ref. 7.)

the experimental arrangements. This experiment of 1958 is the prototype of future inclusive scattering experiments.

In the early sixties the energy of electron beams was increased by a factor of 10, to 6 GeV with the turn-on of the Cambridge Electron Accelerator (CEA) and of the Deutsches Elektronen-Synchrotron (DESY). The inelastic electron scattering work then centered on the dynamics of the production of baryon resonances, as is illustrated in Fig. 2 taken from the work of Cone et al.[7] at CEA and in Fig. 3 taken from that of Albrecht et al.[8] at DESY.

2.2. The SLAC spectrometers

Design of the 20 GeV and 8 GeV spectrometers began soon after construction of the two-mile 20 GeV electron accelerator had started in 1961. These massive and very carefully designed instruments reflect the fact that from the beginning of the project it was anticipated that inclusive scattering would play a dominant role in the experimentation at this machine, characterized by high intensity and small duty cycle.

Panofsky participated in the spectrometer project, and the design owes much to his deep understanding of beam optics. Figures 4 and 5 give an overall view of the 8 GeV and 20 GeV spectrometers, respectively. Figure 6 shows the detector assembly, and Fig. 7 is a photograph of the two spectrometers on the experimental floor.

2.3 The discovery of proton constituents

Inelastic measurements at SLAC began in the summer of 1967. The first important results were the inelastic cross-section at 6° presented at the Vienna meeting in 1968[9] (a week or two after the invasion of Czechoslovakia). The result most relevant to nucleon structure is the one of $d^2\sigma/d\Omega dE'(W,Q^2)$ as a function of Q^2 at W = 2 GeV and 3 GeV, shown in Fig. 8. The Q^2 dependence is quite flat, in marked contrast to the form-factor dependence observed for elastic scattering and resonance production. Just such results had however been predicted by Bjorken for nucleons with 'elementary constituents' in his 1967 Varenna lectures.[10] To quote two of his sentences: "I also think that the problems raised here are quite fundamental, dealing, in what seems to be a direct way, with the question of whether there are any 'elementary constituents' within the nucleon. Use of the lepton as a probe is a unique and possibly powerful way of attacking the problem." Panofsky, in his rapporteur's talk at the Vienna meeting[11] said: "Therefore theoretical speculations are focused on the possibility that these data might give evidence on the behavior of point-like, charged structures within the nucleon."However, the understanding of the impact of these early results at the time of the Vienna Conference was not yet clear. Recalling later the climate of those days, R. Taylor wrote in 1980[12]: "Even by the time of the Liverpool Conference in 1969 many eminent theorists believed that 'Vector Dominance' was the most sensible explanation of the deep inelastic cross-sections. The confirmation of Bjorken's conjecture was gradual rather than a sudden event on a given date." It was probably Feynman who was the first to see the meaning of these first results in the way they are presently understood. Bjorken recalls[13]: "Feynman visited SLAC in the midst of the first scaling data (the stuff presented by Pief at Vienna). He had been doing the parton model for hadron-hadron collisions (there is a Phys. Rev. Letter on that) and

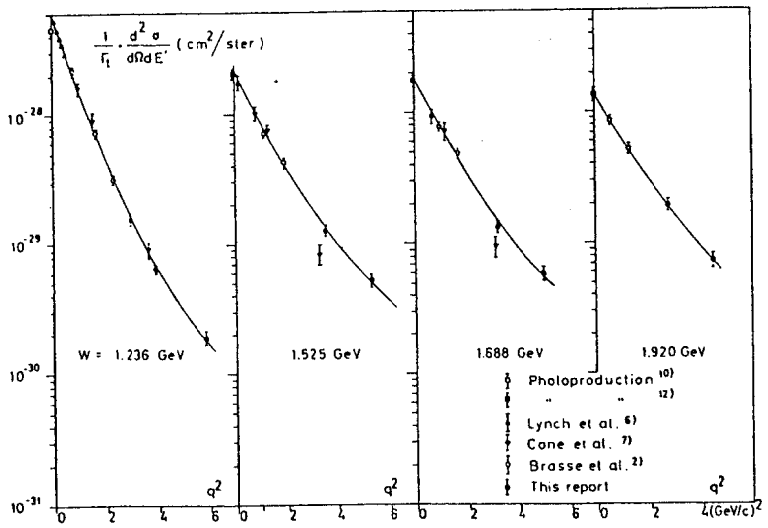

Fig. 3 Form factors for the excitation of baryon resonances. (Ref. 8.)

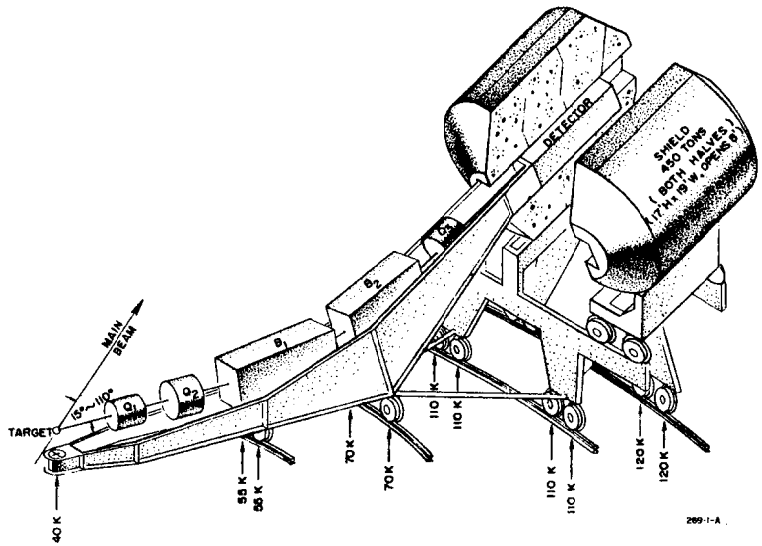

Fig. 4 SLAC 8 GeV spectrometer.

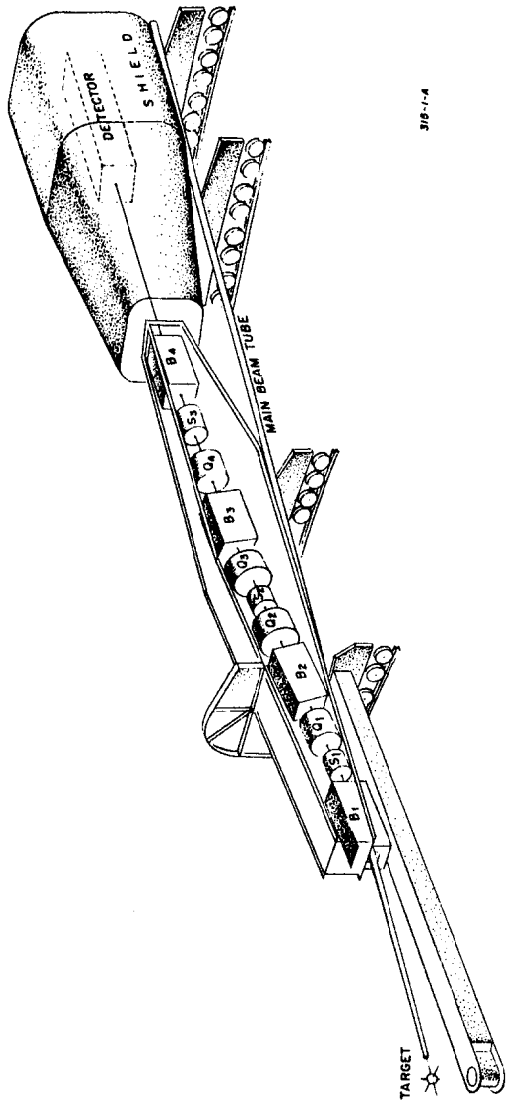

Fig. 5 SLAC 20 GeV spectrometer.

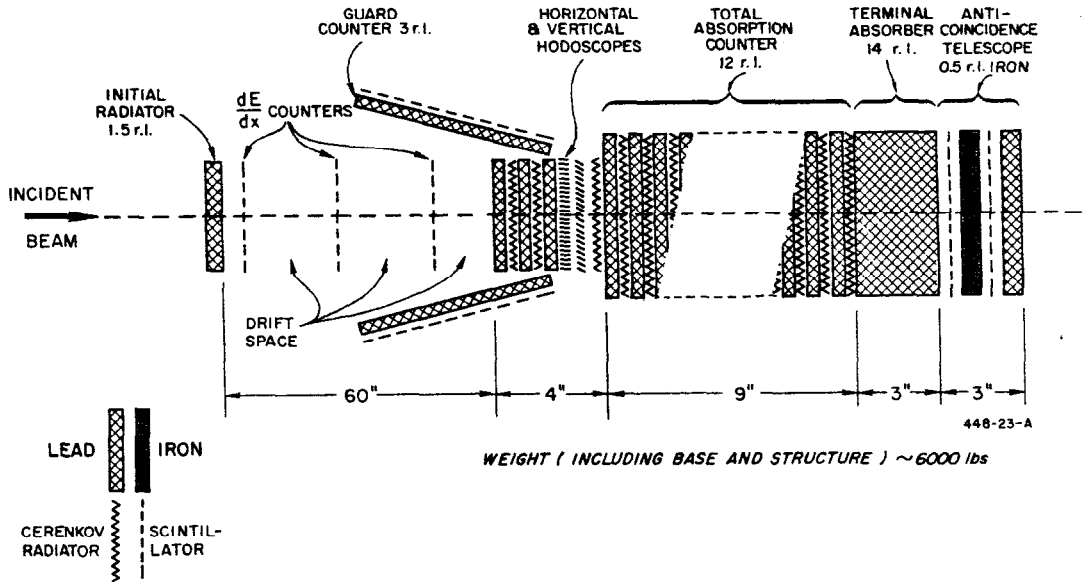

Fig. 6 Detector of SLAC 8 GeV spectrometer.

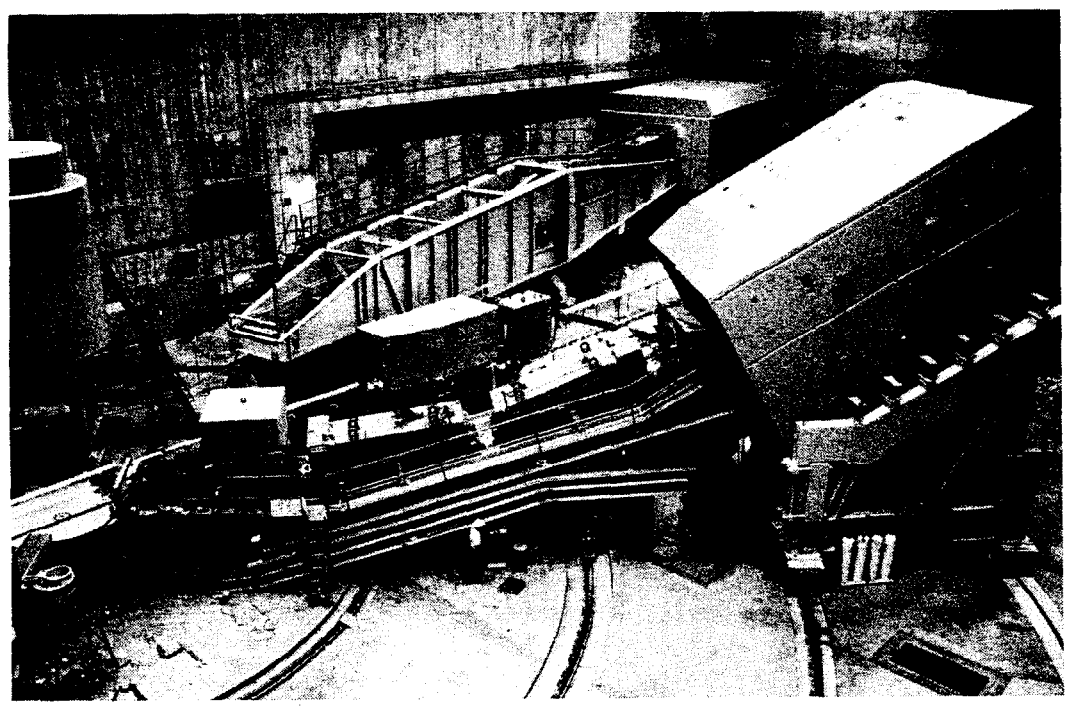

Fig. 7 View of the floor at SLAC with 20 GeV and 8 GeV spectrometers.

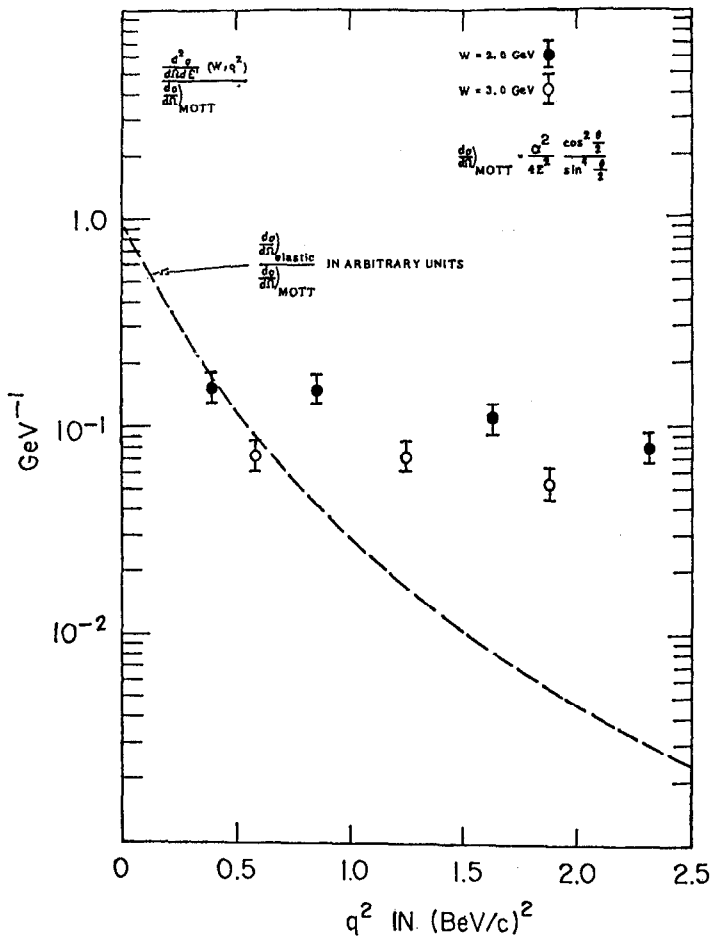

Fig. 8 A plot of $(d^2\sigma/d\Omega dE')/\sigma_{Mott}$ as a function of Q^2 in W bins, presented by the MIT-SLAC group at the Vienna Conference in 1968. First evidence for nucleon point-like constituents.

instantly (i.e. overnight) recognized what was behind the scaling ideas, and went beyond where I had gone (at least in some directions). After he left town, Manny Paschos and I did our paper on partons, emphasizing the (new) idea of deep-inelastic Compton scattering. I expected Feynman to write something on his own, and was too shy to suggest a joint paper or call him up and discuss what to do. Feynman in turn didn't write up his ideas until, really, the Benjamin book 'Photon-Hadron Interactions'. He was of course busy in the meantime."

For mortals the appreciation came more gradually. The 6° data were augmented in 1969 by the 10° data[14] shown in Fig. 9. The data cover a larger Q^2 range, but are still presented in W bins. The scaling variable, W, and the cross-sections in fixed W bins are not expected to be Q^2 independent.

But in 1970, the ideas seem to have crystallized to the presently accepted ones. At the Kiev Conference[15] of that year, data at 6°, 10°, 18°, and 26° were shown, the two structure functions could be separated, and results were for the first time presented in $\omega = 1/x$ bins. As an example, the data at $\omega = 4$ of Fig. 10 show scaling over a large Q^2 domain. The fact that the proton contains quasi-free point-like constituents was established and accepted.

2.4 SLAC structure function determinations

A very brief résumé of definitions and phenomenology is necessary here. Electron-nucleon scattering is presumed to occur via exchange of a photon:

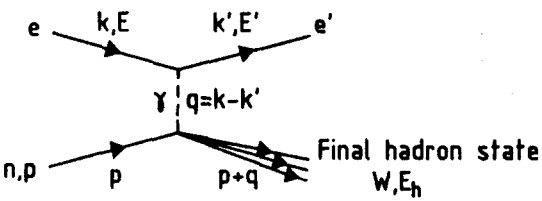

$$Q^2 \equiv -(k-k')^2 = 4EE' \sin^2 \theta/2$$
$$\nu \equiv q \cdot p/M \quad = E - E' = E_h - M$$
$$x \equiv Q^2/2M\nu$$
$$\omega = 1/x$$
$$W^2 \equiv (p+q)^2 .$$

The cross-section can be written in terms of two structure functions, W_1 and W_2, which describe the interaction of the virtual photon with the nucleon:

$$\frac{d^2\sigma}{d\Omega\, dE'} = \sigma_{Mott}\left[W_2(x, Q^2) + 2\ tg^2\ \frac{\theta}{2}\ W_1(x, Q^2)\right].$$

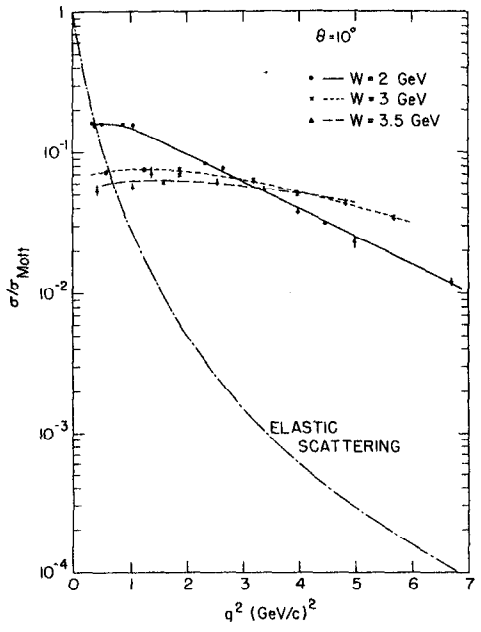

Fig. 9 A plot of $(d^2\sigma/d\Omega dE')/\sigma_M ott$ as a function of Q^2 in W bins; 10° data. (Ref. 15.)

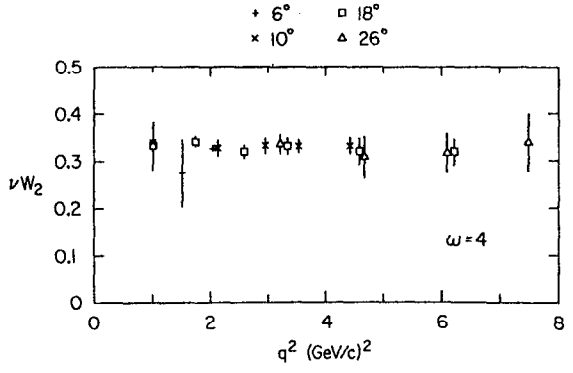

Fig. 10 The structure function, ${}_{\nu}W_2$ at $x = 0.25$, is shown as a function of Q^2, demonstrating scaling. Presented at the 15th Int. Conf. on High Energy Physics, Kiev, 1970. (Ref. 15.)

In place of W_2 and W_1 it is now usual to use $F_2 = \nu W_2$ and $xF_1 = MW_1$. The W_2 and W_1 are related to the scattering cross-sections of longitudinal photons, σ_S, and transverse photons, σ_T, W_2 being proportional to their sum and W_1 to σ_T. The ratio

$$R = \sigma_S/\sigma_T = \left[1 + \frac{2Mx}{\nu}\right]\frac{W_2}{W_1} - 1$$

is expected to be small in the Quark Parton Model (QPM). The R is measured by noting that the cross-section depends linearly on $\epsilon = [1 + (1 + 2\nu^2/Q^2)\,tg^2\,\theta/2]^{-1}$:

$$\frac{d^2\sigma}{d\Omega\,dE'} \propto \left[1 + \epsilon R(x, Q^2)\right] .$$

The earliest presentation of results on R were made at the Kiev Conference of 1970[15] and are shown in Fig. 11. Neutron structure functions were determined by comparing deuterium and hydrogen cross-sections, after correction for the motion of the nucleons in the deuteron. Early results, also shown in Kiev, are reproduced in Fig. 12. In the naïve QPM the ratio is expected to be unity at large ω where the contribution is from the quark-antiquark sea, and 2/3 at small ω, if the up and down quark distributions have the same form. The deviation at small ω, evident in these early data, has been confirmed and must be attributed to differences in the structure functions of up and down quarks in the proton.

The MIT and the SLAC groups went on to complete systematic, precise structure function measurements[16-18] which stand today as landmarks of reliable experimentation. A sample of results is shown in Figs. 13 to 16. Figure 13 of Ref. 16 shows the Q^2 dependence of νW_2 plotted for three sets of 'scaling' variables all reducing to x at large Q^2 and, therefore, equally appropriate. If x is used, scaling is broken; if $x' = x/(1 + xM^2/Q^2)$ is used, scaling is valid. This illustrates that the Q^2 region is too low in Q^2 to permit definitive demonstration of scaling violation. Figure 14 shows a set of precise measurements of σ_n/σ_p reported by the SLAC Group[17]; Fig. 15 shows the latest and most precise R determinations,[18] and Fig. 16, also taken from Ref. 18, is part of a table of the neutron and proton structure functions.

3. NEUTRINO INCLUSIVE SCATTERING

3.1 Phenomenology

The inclusive processes for neutrinos and antineutrinos are, respectively,

$$\nu_\mu + N \to \mu^- + X$$
$$\bar{\nu}_\mu + N \to \mu^+ + X .$$

The cross-sections now require three structure functions. Two of these are the F_1 and F_2 of charged-lepton scattering, the third, F_3, is a consequence of parity violation in the weak

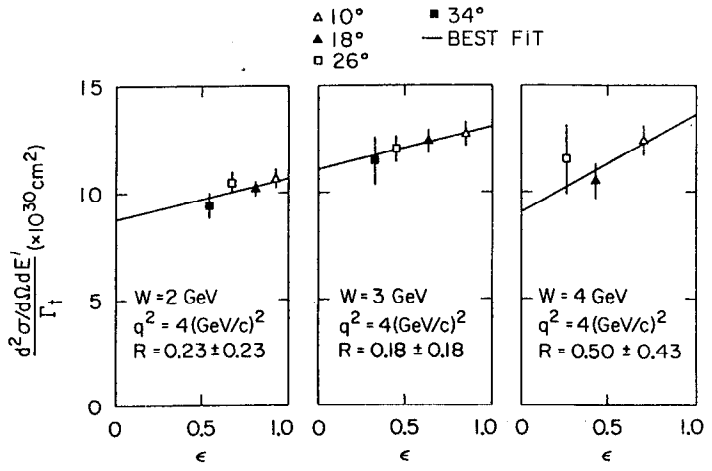

Fig. 11 Early determinations of R, presented in Kiev 1970. (Ref. 15.)

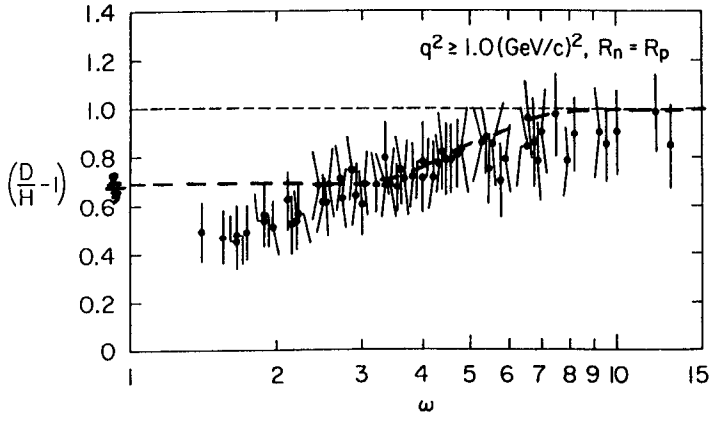

Fig. 12 Comparison of neutron and proton cross-sections as a function of ω. The deviation from the value 2/3 at small ω was the first demonstration that the down and up quark distributions in the proton have different ω dependence. Presented at Kiev 1970. (Ref. 15.)

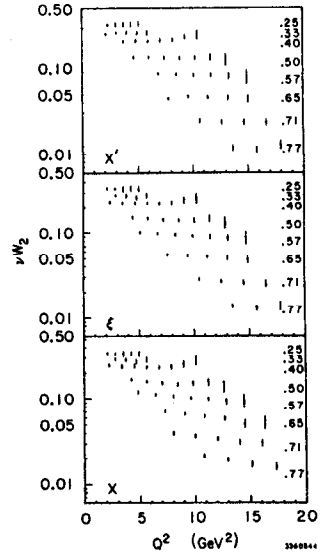

Fig. 13 SLAC measurements of the Q^2 dependence of νW_2, plotted for three different scaling variables: x, $x' = x/(1 + xM^2/Q^2)$ and $\xi = 2x/(1 + \sqrt{1 + 4M^2x^2/Q^2})$. Mestayer Thesis. (Ref. 16.)

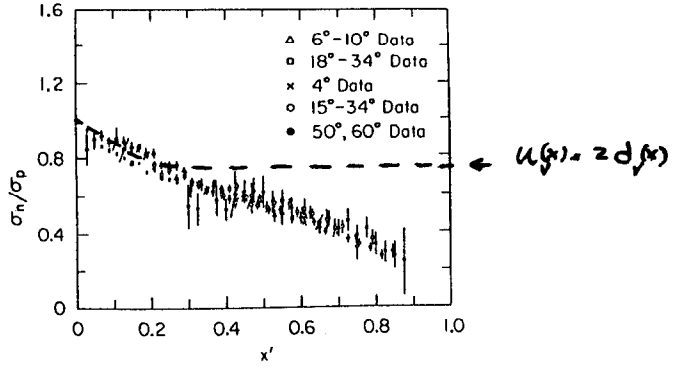

Fig. 14 The ratio of neutron-to-proton cross-sections as a function of $x' = x[1 + (M^2/Q^2)]$. (Ref. 17.)

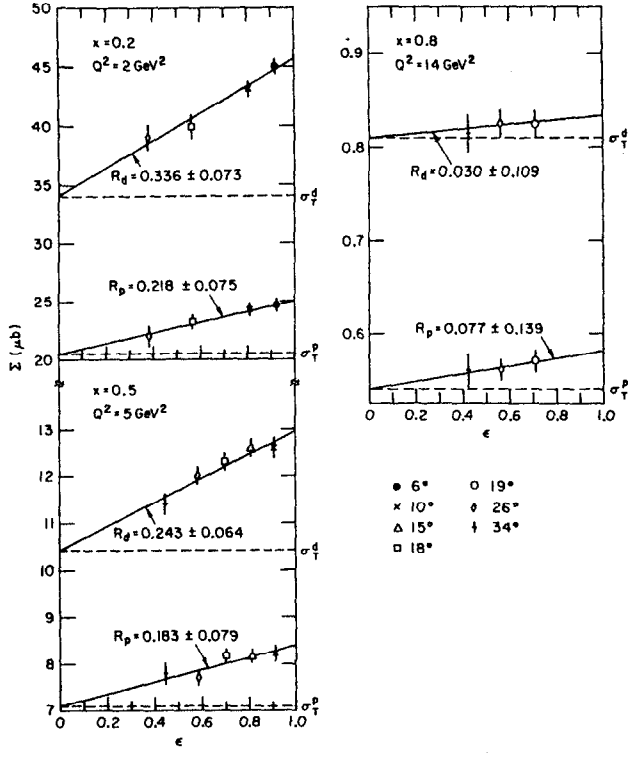

Fig. 15 Determinations of R for three values of x by the MIT group. (Ref. 18.)

x	Q^2 (GeV^2)	$2MW_1^p$	Δ	νW_2^p	Δ	$2MW_1^d$	Δ	νW_2^d	Δ
0.10	1.00	2.7320 ± 0.2435	0.2168	0.3100 ± 0.0086	0.0088	5.3689 ± 0.3524	0.4173	0.5808 ± 0.0126	0.0206
0.10	1.25	2.5293 ± 0.2333	0.2083	0.3291 ± 0.0092	0.0002	5.3258 ± 0.4165	0.4067	0.6120 ± 0.0154	0.0205
0.10	1.50	2.6576 ± 0.1983	0.2238	0.3381 ± 0.0093	0.0095	5.0837 ± 0.3422	0.4125	0.6402 ± 0.0145	0.0215
0.10	2.00	2.5390 ± 0.2401	0.2242	0.3598 ± 0.0172	0.0099	5.1486 ± 0.3443	0.4315	0.6441 ± 0.0248	0.0225
0.10	2.50	2.3170 ± 0.6479	0.2683	0.4295 ± 0.0737	0.0193	5.2006 ± 0.9577	0.5660	0.6649 ± 0.1090	0.0451
0.15	1.00	1.6898 ± 0.1661	0.1565	0.3308 ± 0.0062	0.0098	2.9340 ± 0.2830	0.2900	0.6032 ± 0.0093	0.0217
0.15	1.25	1.9501 ± 0.1395	0.1574	0.3315 ± 0.0074	0.0101	3.1496 ± 0.1921	0.2917	0.6118 ± 0.0103	0.0230
0.15	1.50	2.1034 ± 0.1369	0.1614	0.3283 ± 0.0068	0.0096	3.2092 ± 0.2393	0.2955	0.6216 ± 0.0101	0.0219
0.15	2.00	1.8090 ± 0.0937	0.1404	0.3448 ± 0.0089	0.0102	2.9493 ± 0.2033	0.2427	0.6459 ± 0.0132	0.0236
0.15	2.50	1.7987 ± 0.1546	0.1513	0.3617 ± 0.0162	0.0143	3.0912 ± 0.2153	0.2792	0.6613 ± 0.0223	0.0330
0.15	3.00	1.8201 ± 0.1803	0.1502	0.3544 ± 0.0249	0.0146	3.5006 ± 0.2277	0.2940	0.6407 ± 0.0336	0.0345
0.15	3.50	1.9293 ± 0.2252	0.1548	0.3321 ± 0.0277	0.0147	3.4415 ± 0.2787	0.2923	0.6649 ± 0.0357	0.0369
0.20	1.00	1.5845 ± 0.1287	0.1575	0.3163 ± 0.0049	0.0089	2.7656 ± 0.1911	0.3209	0.5720 ± 0.0073	0.0197
0.20	1.25	1.4686 ± 0.1173	0.1416	0.3288 ± 0.0061	0.0097	2.5827 ± 0.1845	0.2822	0.5880 ± 0.0085	0.0213
0.20	1.50	1.2762 ± 0.1070	0.1205	0.3399 ± 0.0056	0.0098	2.2135 ± 0.1557	0.2358	0.6000 ± 0.0076	0.0212
0.20	2.00	1.4645 ± 0.0710	0.1029	0.3333 ± 0.0058	0.0093	2.4341 ± 0.1128	0.1784	0.6076 ± 0.0077	0.0205
0.20	2.50	1.6122 ± 0.0776	0.1067	0.3270 ± 0.0076	0.0098	2.5299 ± 0.1466	0.1673	0.5986 ± 0.0106	0.0221
0.20	3.00	1.5177 ± 0.0948	0.1086	0.3394 ± 0.0124	0.0124	2.5064 ± 0.1276	0.1996	0.6113 ± 0.0169	0.0277
0.20	3.50	1.4257 ± 0.1150	0.1036	0.3457 ± 0.0171	0.0132	2.2603 ± 0.1571	0.1900	0.6367 ± 0.0236	0.0303
0.20	4.00	1.4912 ± 0.0967	0.1021	0.3247 ± 0.0156	0.0130	2.2965 ± 0.1345	0.1844	0.6385 ± 0.0218	0.0312
0.25	1.00	1.0798 ± 0.1275	0.1642	0.3184 ± 0.0046	0.0087	1.8854 ± 0.1832	0.3399	0.5509 ± 0.0066	0.0186
0.25	1.25	1.3236 ± 0.1200	0.1383	0.3112 ± 0.0046	0.0088	2.1859 ± 0.1662	0.2872	0.5500 ± 0.0067	0.0191
0.25	1.50	1.1189 ± 0.0962	0.1162	0.3188 ± 0.0042	0.0088	1.8561 ± 0.1320	0.2364	0.5575 ± 0.0058	0.0189
0.25	2.00	1.1714 ± 0.0682	0.0858	0.3253 ± 0.0047	0.0087	1.8545 ± 0.0985	0.1508	0.5623 ± 0.0063	0.0184
0.25	2.50	1.1623 ± 0.0920	0.0872	0.3195 ± 0.0072	0.0095	1.8625 ± 0.1642	0.1633	0.5634 ± 0.0100	0.0206
0.25	3.00	1.1888 ± 0.0612	0.0787	0.3211 ± 0.0086	0.0100	1.9217 ± 0.0848	0.1339	0.5559 ± 0.0113	0.0207
0.25	4.00	1.1873 ± 0.0792	0.0720	0.3082 ± 0.0129	0.0100	1.9741 ± 0.1030	0.1325	0.5493 ± 0.0176	0.0223
0.25	5.00	1.2402 ± 0.0653	0.0716	0.2959 ± 0.0112	0.0103	2.0154 ± 0.0838	0.1273	0.5295 ± 0.0142	0.0236
0.33	1.50	0.7480 ± 0.1035	0.1193	0.2916 ± 0.0038	0.0079	1.2260 ± 0.1298	0.2470	0.4827 ± 0.0053	0.0163
0.33	2.00	0.8939 ± 0.0505	0.0677	0.2794 ± 0.0033	0.0071	1.4293 ± 0.0659	0.1277	0.4676 ± 0.0046	0.0146
0.33	2.50	0.8863 ± 0.0734	0.0749	0.2756 ± 0.0043	0.0076	1.5366 ± 0.1389	0.1451	0.4559 ± 0.0062	0.0157
0.33	3.00	0.8064 ± 0.0316	0.0467	0.2799 ± 0.0039	0.0070	1.2626 ± 0.0401	0.0777	0.4622 ± 0.0051	0.0145
0.33	4.00	0.8449 ± 0.0331	0.0449	0.2674 ± 0.0057	0.0072	1.2266 ± 0.0442	0.0733	0.4534 ± 0.0080	0.0148
0.33	5.00	0.8084 ± 0.0452	0.0435	0.2600 ± 0.0080	0.0078	1.1362 ± 0.0569	0.0750	0.4590 ± 0.0106	0.0164
0.33	6.00	0.5898 ± 0.0765	0.0312	0.3114 ± 0.0243	0.0089	1.2554 ± 0.0927	0.0603	0.4201 ± 0.0301	0.0092
0.33	7.00	0.6487 ± 0.0857	0.0323	0.2795 ± 0.0336	0.0063	1.2306 ± 0.1015	0.0588	0.4124 ± 0.0401	0.0094
0.40	2.00	0.6927 ± 0.0464	0.0578	0.2464 ± 0.0028	0.0062	1.0314 ± 0.0573	0.1054	0.3965 ± 0.0038	0.0118
0.40	3.00	0.6342 ± 0.0250	0.0356	0.2303 ± 0.0032	0.0055	0.9751 ± 0.0299	0.0594	0.3732 ± 0.0042	0.0109
0.40	4.00	0.5570 ± 0.0252	0.0309	0.2331 ± 0.0041	0.0057	0.8831 ± 0.0302	0.0516	0.3700 ± 0.0054	0.0117
0.40	5.00	0.5683 ± 0.0229	0.0272	0.2259 ± 0.0049	0.0054	0.8589 ± 0.0277	0.0433	0.3610 ± 0.0062	0.0097
0.40	6.00	0.5731 ± 0.0228	0.0259	0.2118 ± 0.0044	0.0052	0.8422 ± 0.0257	0.0421	0.3521 ± 0.0054	0.0099
0.40	7.00	0.5430 ± 0.0280	0.0236	0.2091 ± 0.0082	0.0056	0.8108 ± 0.0314	0.0358	0.3501 ± 0.0098	0.0079
0.40	8.00	0.4982 ± 0.0261	0.0218	0.2170 ± 0.0088	0.0058	0.7907 ± 0.0290	0.0343	0.3399 ± 0.0105	0.0079
0.40	9.00	0.4746 ± 0.0401	0.0205	0.2104 ± 0.0202	0.0048	0.7868 ± 0.0476	0.0335	0.3289 ± 0.0246	0.0074
0.50	3.00	0.4129 ± 0.0194	0.0248	0.1714 ± 0.0021	0.0040	0.6160 ± 0.0228	0.0417	0.2879 ± 0.0028	0.0075
0.50	4.00	0.3439 ± 0.0167	0.0182	0.1677 ± 0.0028	0.0037	0.5286 ± 0.0188	0.0302	0.2558 ± 0.0036	0.0072
0.50	5.00	0.3166 ± 0.0164	0.0153	0.1593 ± 0.0029	0.0033	0.4644 ± 0.0183	0.0235	0.2454 ± 0.0036	0.0056
0.50	6.00	0.3181 ± 0.0134	0.0136	0.1505 ± 0.0027	0.0033	0.4616 ± 0.0156	0.0217	0.2380 ± 0.0034	0.0060
0.50	7.00	0.3014 ± 0.0136	0.0135	0.1453 ± 0.0029	0.0031	0.4365 ± 0.0160	0.0210	0.2279 ± 0.0033	0.0055
0.50	8.00	0.2974 ± 0.0159	0.0115	0.1392 ± 0.0047	0.0026	0.4080 ± 0.0176	0.0183	0.2285 ± 0.0056	0.0042
0.50	10.00	0.2555 ± 0.0160	0.0112	0.1429 ± 0.0087	0.0030	0.4063 ± 0.0174	0.0163	0.2124 ± 0.0075	0.0045
0.50	12.00	0.2501 ± 0.0175	0.0095	0.1379 ± 0.0083	0.0033	0.3823 ± 0.0205	0.0143	0.2084 ± 0.0104	0.0048
0.60	5.00	0.1736 ± 0.0114	0.0082	0.1023 ± 0.0018	0.0020	0.2902 ± 0.0130	0.0126	0.1470 ± 0.0023	0.0028
0.60	6.00	0.1601 ± 0.0085	0.0072	0.0983 ± 0.0018	0.0020	0.2642 ± 0.0094	0.0111	0.1395 ± 0.0021	0.0030
0.60	7.00	0.1624 ± 0.0070	0.0068	0.0900 ± 0.0015	0.0020	0.2338 ± 0.0078	0.0106	0.1319 ± 0.0017	0.0033
0.60	8.00	0.1484 ± 0.0081	0.0055	0.0884 ± 0.0022	0.0017	0.2142 ± 0.0093	0.0078	0.1290 ± 0.0026	0.0034

Fig. 16 Example of structure function determinations by the MIT group. (Table taken from Ref. 18.)

interaction. The sum of the two cross-sections has the same form as charged lepton scattering:

$$\frac{d^2\sigma^{\nu}}{dx\,dy} + \frac{d^2\sigma^{\bar{\nu}}}{dx\,dy} = \frac{G^2ME}{\pi} F_2(x, Q^2)\left[1 + (1-y)^2 - y^2R'\right] ,$$

whereas their difference gives directly F_3:

$$\frac{d^2\sigma^{\nu}}{dx\,dy} - \frac{d^2\sigma\bar{\nu}}{dx\,dy} = \frac{G^2ME}{\pi} xF_3(x, Q^2)\left[1 - (1-y)^2\right] .$$

Here

$$R' \equiv 1 - \frac{2xF_1}{F_2} \simeq \frac{R}{R+1} \simeq R \text{ for small } R$$

and

$$y = \frac{\nu}{E} \simeq \frac{E_h}{E} .$$

In the QPM, the inclusive variable $x = Q^2/2M\nu$ can be understood as the fraction of the nucleon momentum (in a frame in which the nucleon is moving rapidly) which the struck *quark carries. For I = 0 nuclei*

$$2\,xF_1^{\nu} = F_2^{\nu} = q + \bar{q} \quad \text{and} \quad xF_3 = q - \bar{q}$$

where

q = $u(x) + d(x) + s(x) + c(x)$ is the total quark distribution,

$\bar{q}$ = $\bar{u}(x) + \bar{d}(x) + \bar{s}(x) + \bar{c}(x)$ is the total antiquark distribution, and

$q - \bar{q} = \left[u(x) - \bar{u}(x)\right] + \left[d(x) - \bar{d}(x)\right] = q_v$, the valence quark distribution.

In neutrino inclusive scattering the quark, antiquark, and valence quark distributions are separately measurable.

3.2 Early total cross-sections and structure functions

The first neutrino and antineutrino total cross-sections were published in 1973,[19] a few years after the SLAC discovery of scaling. The measurements were made at the CERN 24 GeV Proton Synchrotron, using the large heavy-liquid bubble chamber 'Gargamelle'. The results (Fig. 17) exhibit the proportionality with neutrino energy, which is a consequence of the scaling of the structure functions.

The first neutrino structure function publication[20] followed in 1975. The result (Fig. 18), based on 200 neutrino and 29 antineutrino events, is the first measurement of the

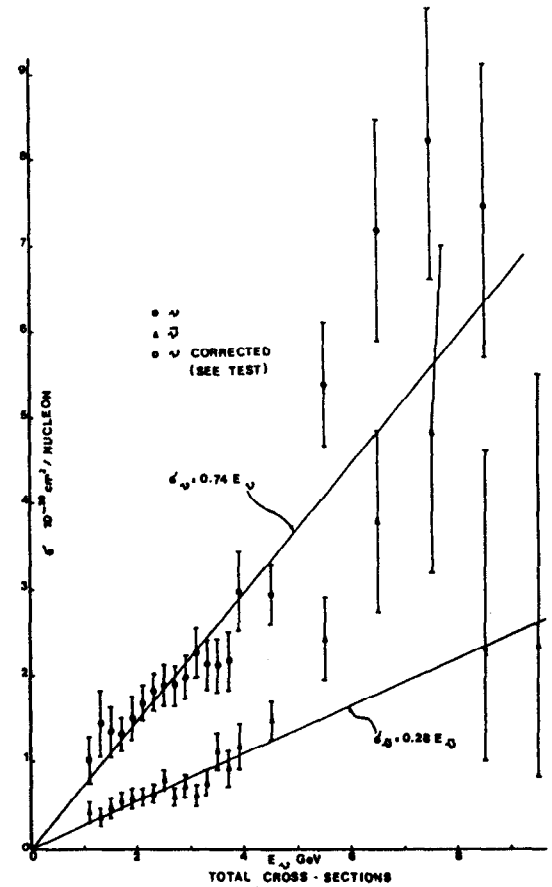

Fig. 17 Neutrino–nucleon total cross-sections as a function of neutrino total energy. (Ref. 19.)

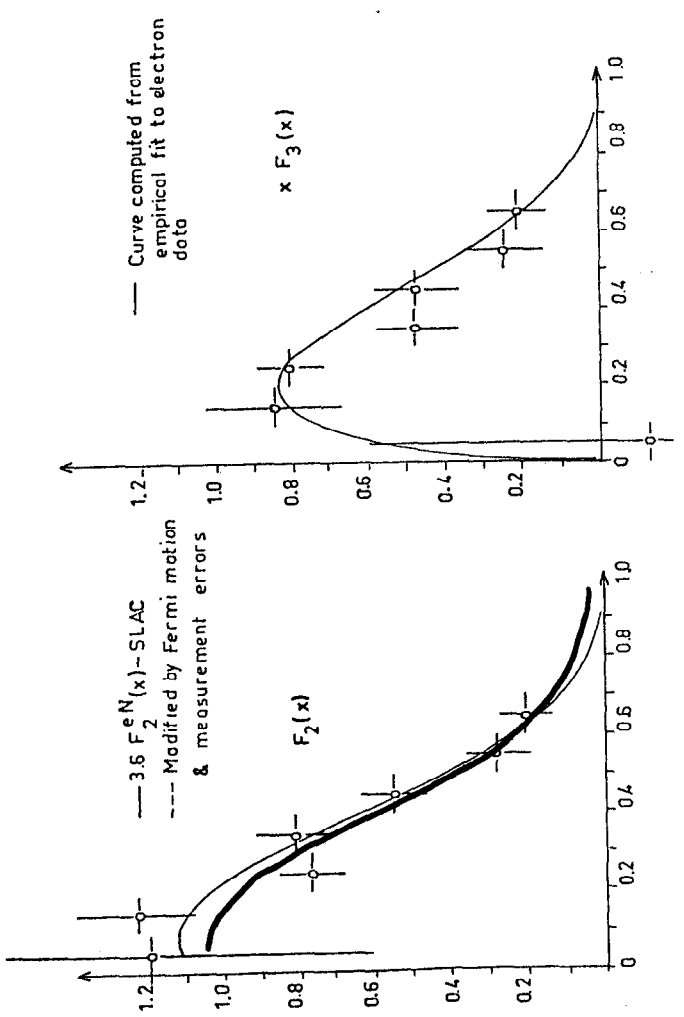

Fig. 18 Early neutrino structure-function measurements in Gargamelle. (Ref. 20.)

valence quark distribution $xF_3(x)$. The results for $F_2(x)$ were compared with the SLAC electron-deuteron scattering (ed) results. In the QPM one expects

$$\frac{F_2(ed)/nucleon}{F_2(\nu N)/nucleon} = \frac{5}{18} .$$

The agreement is an important success of the model.

3.3 Neutrino experimentation in the few hundred GeV range

With the advent of the 400 GeV proton accelerators at Fermilab and CERN, neutrino experimentation took a big leap forward, in part because the higher energies were more amenable to electronic techniques and very massive electronic detectors could be constructed, in part because the cross-sections are proportional to energy, and in part because beam intensities became greater as accelerator technology advanced. In Fig. 19 a photograph is shown of the two large detectors installed at CERN: The CERN-Dortmund-Heidelberg-Saclay (CDHS) detector in front and the CERN-Hamburg-Amsterdam-Rome-Moscow (CHARM) detector in the rear. The CDHS detector weighs ~ 1200 t, of which 500-800 can be used as fiducial target mass. It is constructed of modules, each consisting of 15 magnetized iron plates, 5 cm thick, interleaved with scintillator strips. These modules have a triple function: neutrino target, hadron calorimeter, and muon spectrometer. The muon track is measured in triple-plane drift chambers which are installed between the iron modules. Figure 20 shows an artist's view of the detector and Fig. 21 the computer reconstruction of an event.

The impact of the results which have been accumulated since the SPS turn-on in 1976 and which concern nucleon structure are twofold: One aspect is the independent determination of F_2 and xF_3 or, equivalently, the quark and antiquark distributions, and the consequent deeper probing of the QPM. The second aspect is the demonstration and detailed measurement of the scaling violations of the structure function at large Q^2, and the consequent check of quantum chromodynamics (QCD) and the determination of the strong coupling constant and the gluon structure function.

3.4 Structure function and QPM

Among the results which bear on the QPM of nucleon structure one may mention the following:

i) The total neutrino and antineutrino cross-sections are proportional to the neutrino energy in the laboratory system. Recent CDHS results[21,22] shown in Fig. 22, demonstrate scaling over a larger Q^2 range. The ratio of the two cross-sections has an important significance in the QPM; from it the ratio of the momenta carried by antiquarks and quarks in the nucleon can be found:

$$\frac{\text{Antiquarks}}{\text{Quarks}} = \frac{\sigma^{\bar{\nu}}/\sigma^{\nu} - \frac{1}{3}}{1 - \frac{1}{3}\sigma^{\bar{\nu}}/\sigma^{\nu}} ,$$

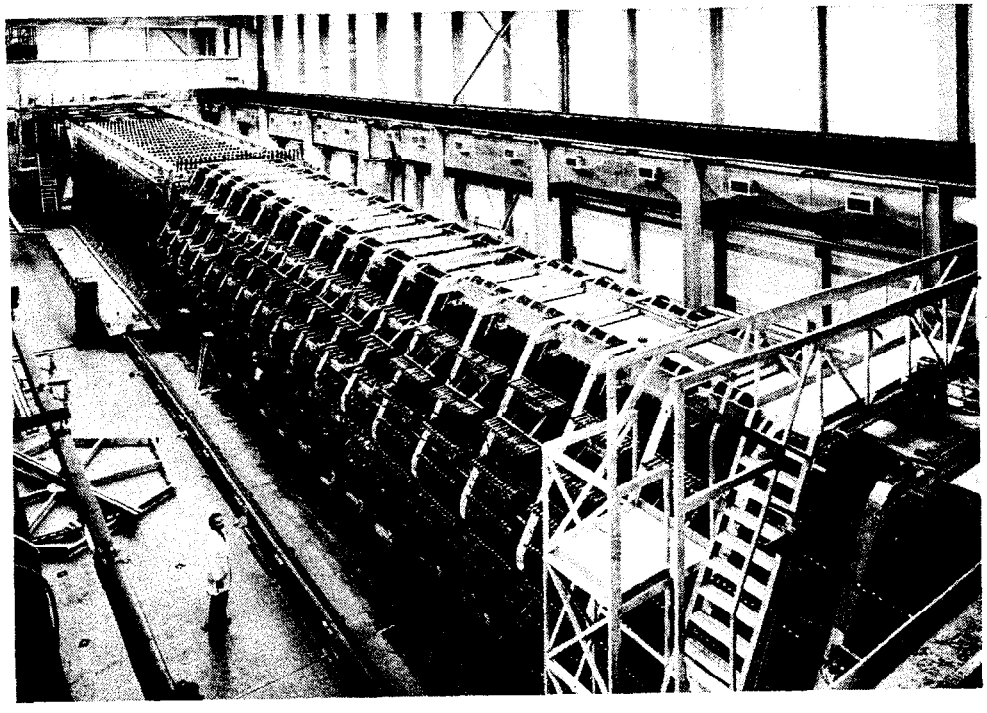

Fig. 19 Photograph of the two electronic neutrino detectors installed at the CERN SPS.

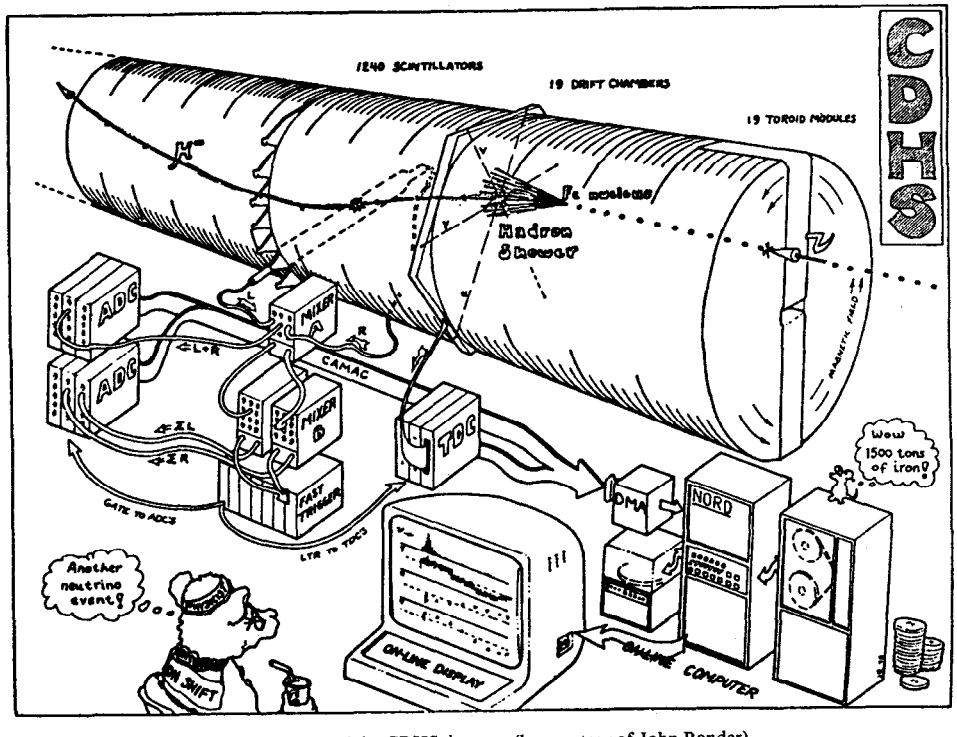

Fig. 20 Artist's view of the CDHS detector (by courtesy of John Rander).

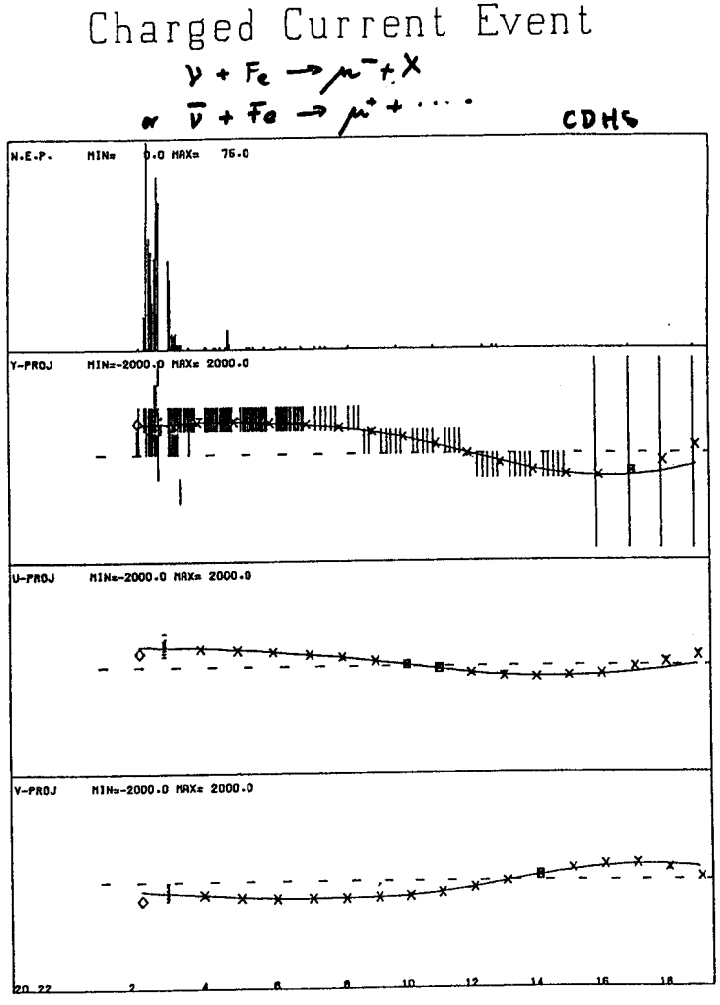

Fig. 21 Typical charged-current event in the CDHS detector. The top view shows the hadron energy observed as pulse height in succeeding scintillator planes. The next lower view is a horizontal projection, showing scintillator hits and drift-chamber positions. The following two views show the drift chamber positions in the other wire planes at ±60°. The muon trajectory is computer reconstructed.

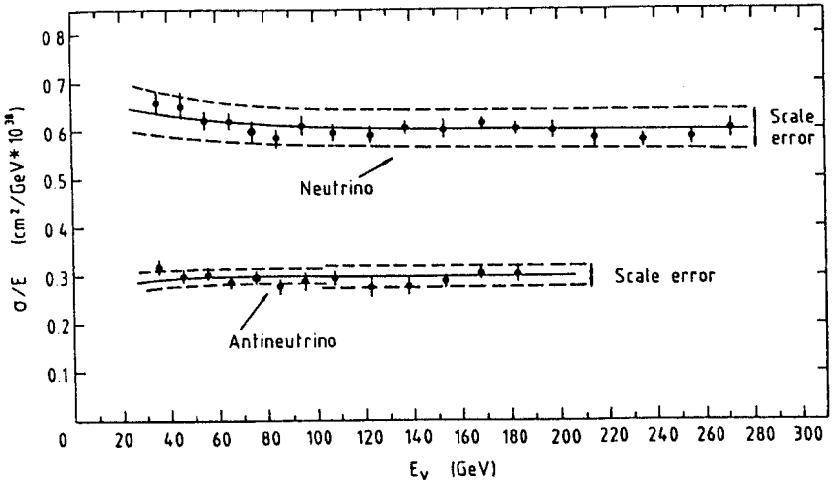

Fig. 22 Neutrino and antineutrino total cross-sections as a function of neutrino energy (CDHS). (Ref. 21.)

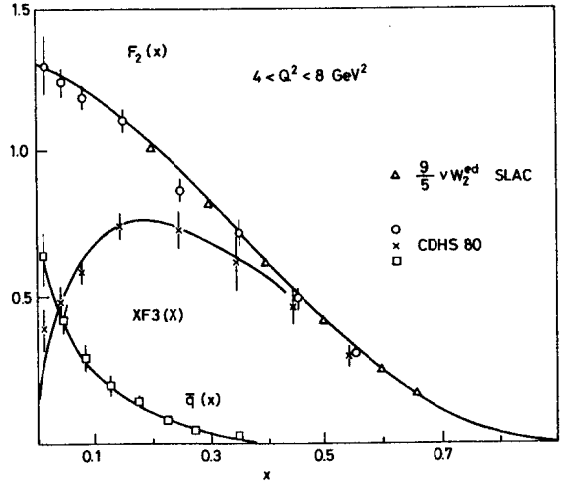

Fig. 23 The $F_2(x)$ (total quark), the $xF_3(x)$ (valence quark), and the antiquark structure functions (Ref. 22). The $F_2^{\nu}(x)$ is compared with $(18/5)F_2^{ed}(x)$ measured at SLAC.

the measured ratio [21] σ^0/σ^ν of 0.48 corresponds to an antiquark/quark ratio of 0.18.

ii) The structure functions $F_2^\nu(x)$ has the same shape as $F_2^{\ell\pm}(x)$ and the magnitudes are related as expected in the QPM by the ratio 18/5. SLAC and CDHS results for $F_2(x)$ are compared in Fig. 23.

iii) The integral $\int_0^1 xF_3(x)dx/x$ is expected to be equal to 3, the number of valence quarks. This is in agreement with experimental results.[21,23]

iv) The valence quark structure $xF_3(x)$ goes towards zero as x goes to zero, and the antiquark structure function is concentrated at small x, as shown in Fig. 23.

v) The ratio $R'(x)$ is small[24] (Fig. 24).

3.5 Q^2 dependence of structure functions and quantum electrodynamics

Following the success of the electroweak gauge theory, the gauge theory of colored quarks was developed.[25] Although the structure function could not, and still cannot, be calculated in this theory, because in this energy domain perturbation approximations fail, the theory has the remarkable property that with increasing Q^2 the effective coupling constant decreases, such that perturbation calculations become reliable at large Q^2. The theory predicts deviations from scaling which are calculable at sufficiently high Q^2. These scaling violations provide a unique possibility for the quantitative confrontations of QCD theory with experiment.

The most direct check is provided by $xF_3(x,Q^2)$ since the equations[26] are homogeneous in xF_3, involving only a single free parameter, the Λ of the running strong coupling constant:

$$\alpha_S = \frac{12\pi}{(33-2f)\ \ln Q^2/\Lambda^2}\ .$$

The equations for $F_2(x,Q^2)$ and $\bar{q}(x,Q^2)$ couple the Q^2 evolutions of these functions to the gluon structure function $G(x,Q^2)$. This makes the comparison of theoretical and experimental Q^2 evolution less direct, but alternatively the experimental Q^2 evolution of $F_2(x,Q^2)$ and $\bar{q}(x,Q^2)$ can be used on the basis of the theory to determine $G(x,Q^2)$.

In Figs. 25, 26, and 27 the CDHS results[22] for $xF_3(x,Q^2)$, $F_2(x,Q^2)$, and $\bar{q}(x,Q_2)$ are shown, together with QCD fits. The simple QCD first- and second-order equations give a good fit to experiment with $\Lambda = (0.2 \pm 0.1)(\mathrm{GeV/c})^2$ and with the gluon distribution[27] shown in Fig. 28. This represents the earliest quantitative test of QCD and may still be the best, although many other confirmations, especially from quark production in e^+e^- collisions, give strong support to the validity of QCD.

4. MUON–HADRON INCLUSIVE SCATTERING

The first experiments at high Q^2 to provide evidence of scaling violations were the muon inclusive scattering experiments of Chang et al. at FNAL.[28] In the following, however, we refer to the subsequent more precise experiments of the European Muon Collaboration (EMC)[29] which take advantage of the better muon beams available at CERN and a very powerful detector (Fig. 29).

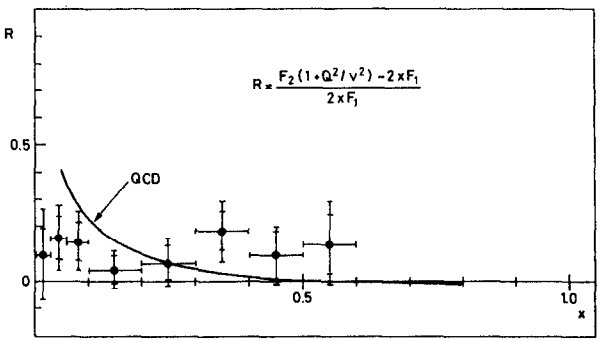

Fig. 24 The ratio $R'(x)$ as a function of x. (Ref. 24.)

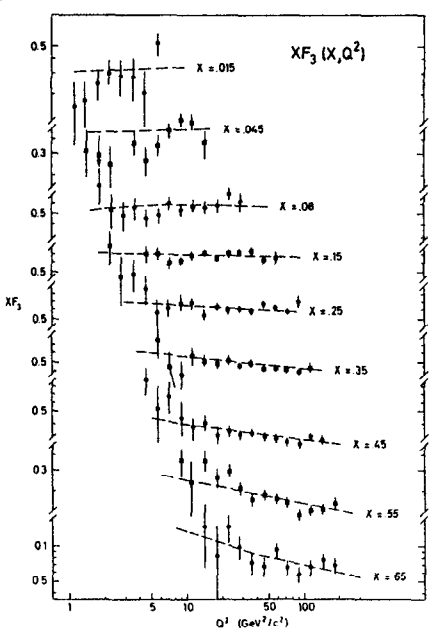

Fig. 25 The structure function $xF_3(x,Q^2)$ as a function of Q^2. (Ref. 21.)

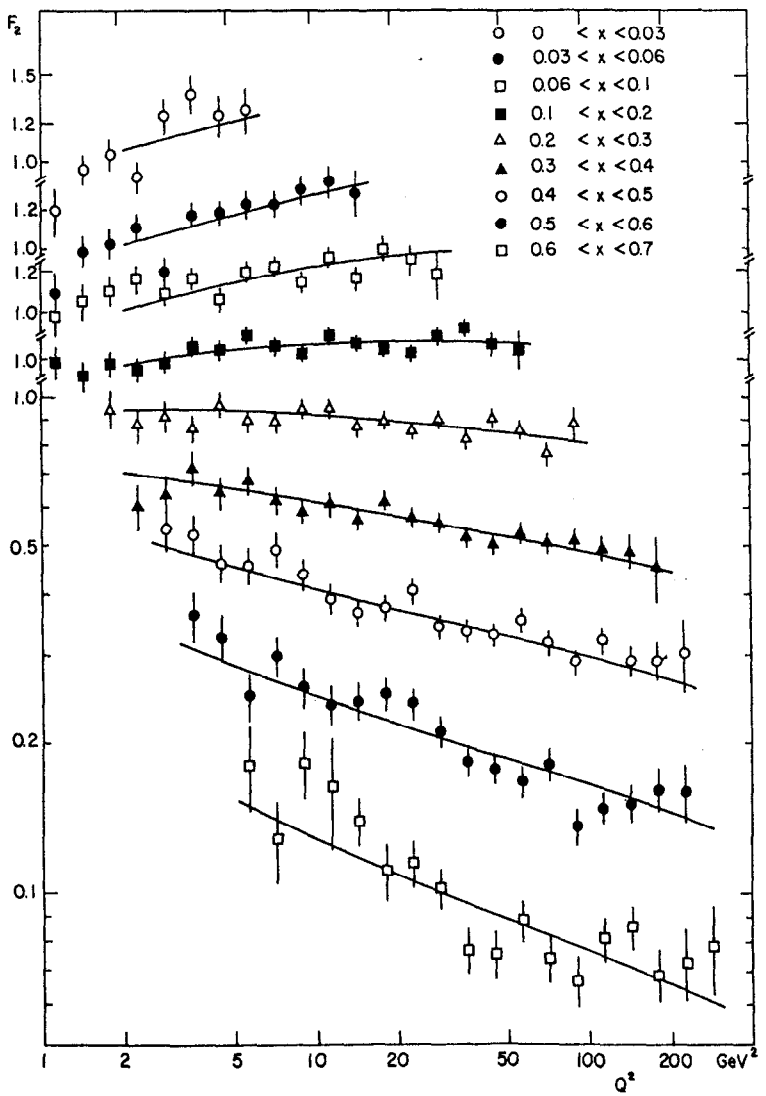

Fig. 26 The structure function $F_2(x, Q^2)$ as a function of Q^2. (Ref. 21.)

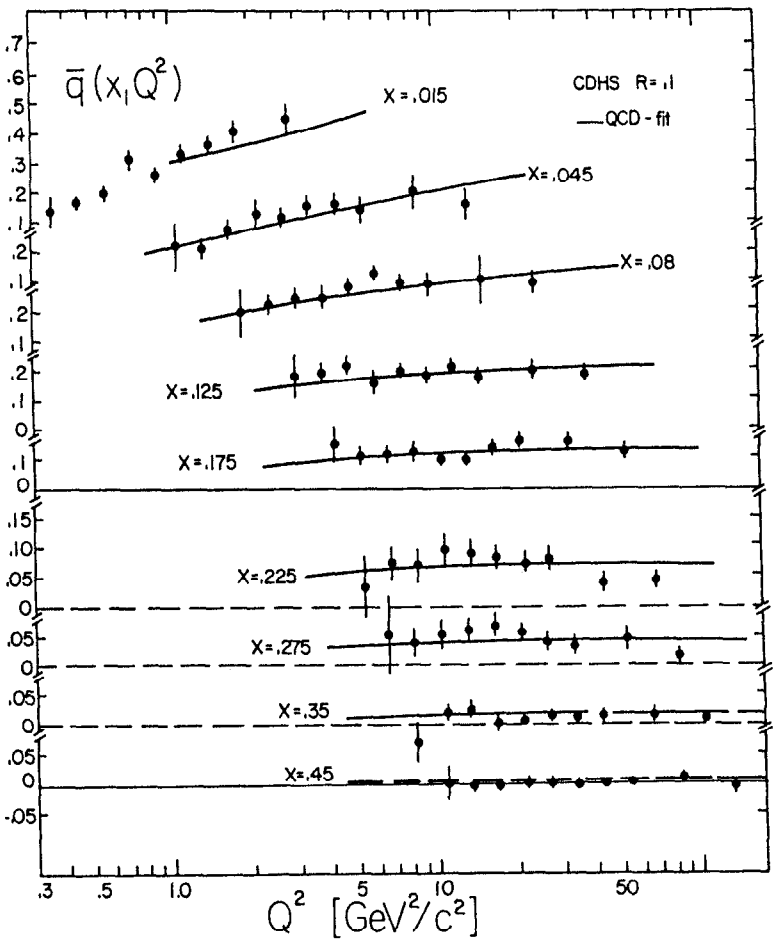

Fig. 27 A plot of $\bar{q}(x, Q^2)$ as a function of Q^2. (Ref. 21.)

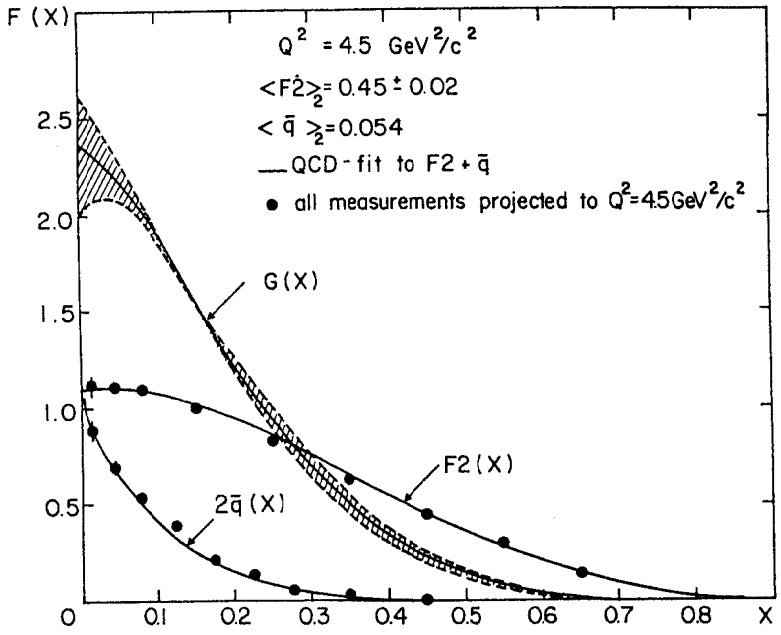

Fig. 28 Gluon structure function as determined from the Q^2 evolution of F_2 and $\bar{q}$. (Ref. 27.)

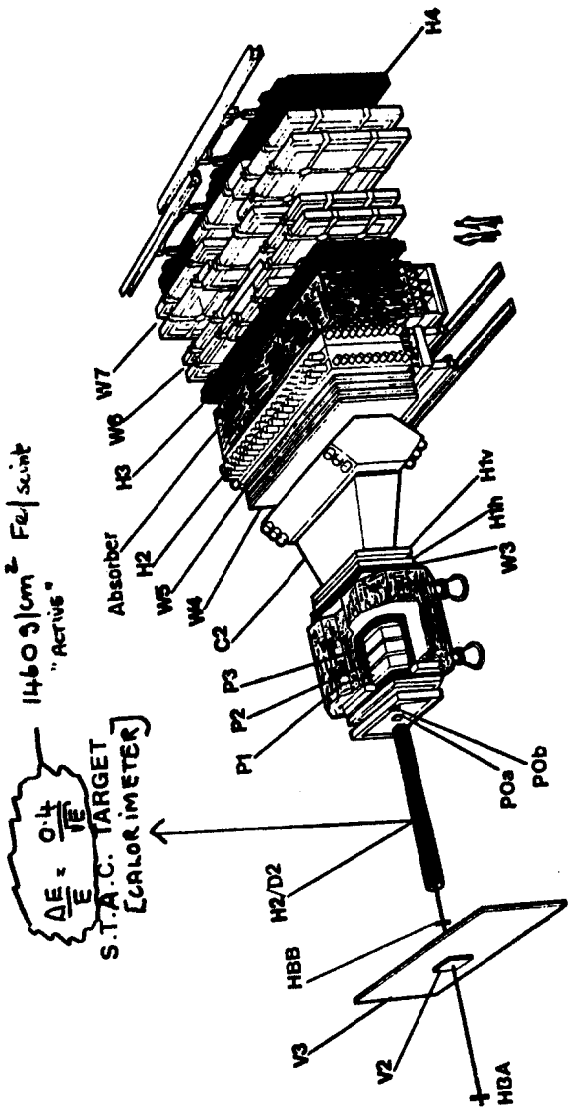

FORWARD SPECTROMETER [E.M.C]

Fig. 29 EMC apparatus.

The most recent EMC results[30] on scaling violations of the structure function $F_2(x, Q^2)$ in iron are shown in Fig. 30. They are statistically superior to the neutrino results; the agreement, after the QPM scale factor of 18/5 is applied, is excellent, as can be seen in Figs. 31 and 32. The structure function $F_2(x, Q^2)$ for hydrogen is show in Fig 33. The QCD analysis of the hydrogen and iron data gives good fit, [31] with $\Lambda_{MS} = 175^{+100}_{-50} MeV$.

Deuterium structure functions have also been measured. Comparison of iron and deuterium structure functions showed differences[32] of the order of 10-20%, which came as a surprise and must be attributed to effects of nuclear binding on the nucleon quarks distributions. The EMC results for $F_2^{Fe}/F_2^{D_2}$ as well as subsequent SLAC results[33] and a corresponding neutrino result:

$$\frac{2}{56}\left(\frac{d\sigma^{\nu Fe}}{dx} + \frac{d\sigma^{\bar{\nu} Fe}}{dx}\right) \Big/ \left(\frac{d\sigma^{\nu p}}{dx} + \frac{d\sigma^{\bar{\nu} p}}{dx}\right)$$

measured by CDHS,[34] are shown in Fig. 34. The rise of the SLAC results at very large x is probably due to the Fermi motion in iron. The EMC effect is confirmed at intermediate x, but not at small x. The effect is not yet well understood, either experimentally or theoretically, but is of substantial interest since it offers the possibility of studying new aspects of the behavior of multiquark systems.

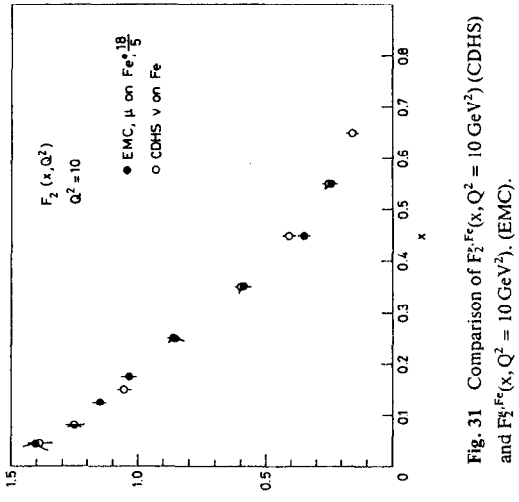

Fig. 31 Comparison of $F_2^{\mu Fe}(x, Q^2 = 10\ GeV^2)$ (CDHS) and $F_2^{\mu Fe}(x, Q^2 = 10\ GeV^2)$. (EMC).

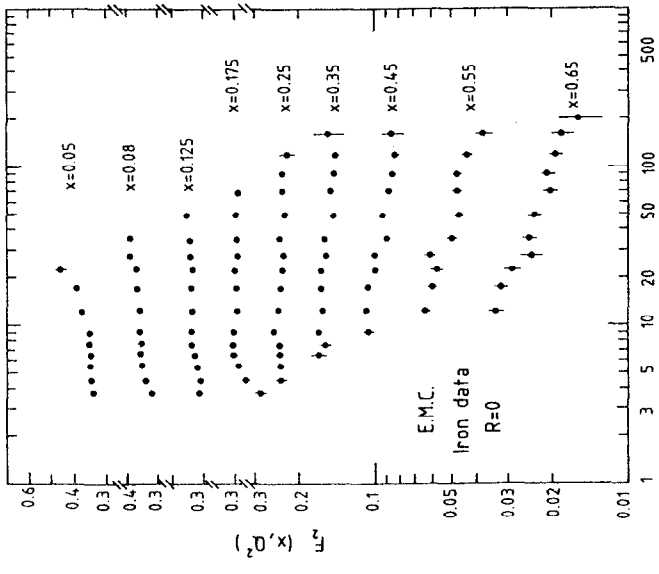

Fig. 30 The structure function $F_2^{\mu, Fe}(x, Q^2)$ from the EMC experiment is shown as a function of Q^2. (Ref. 30.)

5. INCLUSIVE SCATTERING AND NEUTRAL CURRENTS

5.1 Discovery of neutral currents

In 1972 the 'Weinberg Model' of electroweak interactions had reached its full development.[35] For the first time a renormalizable theory of the weak interaction was proposed which moreover unified the weak and electromagnetic interactions. The weak forces were transmitted by intermediate bosons, but in addition to the charged-current processes, neutral-current processes such as $\nu + N \to \nu + X$ and $\bar{\nu} + N \to \bar{\nu} + X$ were predicted as a consequence of the exchange of a neutral boson, Z^0. However, neutral-current reactions had not been seen, despite the fact that the weak interaction had been extensively studied. The Glashow-Iliopoulos-Maiani model[36] provided a way out, by eliminating flavor-changing neutral currents, at the expense of introducing a new particle called charm. The remaining, flavor-conserving, neutral current could have been investigated in the earlier neutrino experiments, but in those days no one imagined neutral currents. In 1972 Gargamelle, the large heavy-liquid bubble chamber 4.8 m long and 1.85 m in diameter, built at ORSAY under the direction of A. Lagarrigue, had just been exposed to both neutrino and antineutrino beams at CERN. Responding to the prompting of the theorists, the group searched for muonless events. The publication appeared in 1973.[37] The demonstration rested on the uniformity of the distribution of the muonless events along the beam direction in the bubble chamber, as can be seen in Fig. 35a and d, whereas neutron background would be expected to decay longitudinally, as in Fig. 35g and h. From the observed event ratios of neutral to charged currents, a Weinberg angle $\sin^2 \Theta_w$ between 0.3 and 0.4, not too far from the presently accepted value of 0.22 was

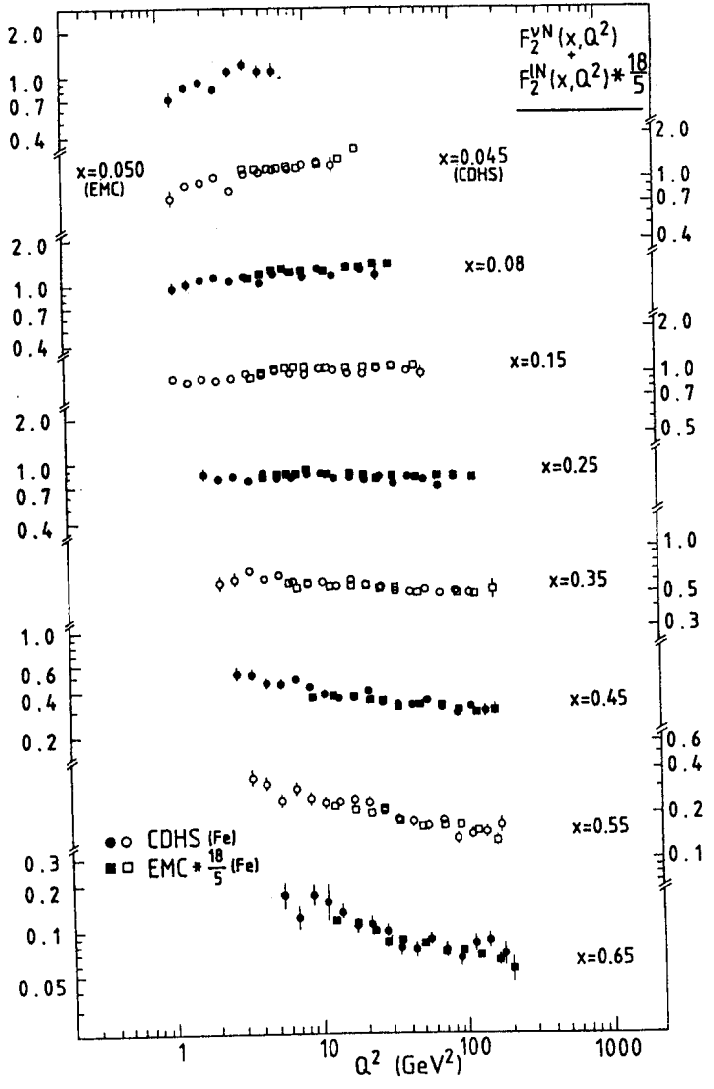

Fig. 32 Comparison of Q^2 dependence of $F_2^{\nu,Fe}(x,Q^2)$ (CDHS) and $F_2^{\ell,Fe}(x,Q^2)$ (EMC).

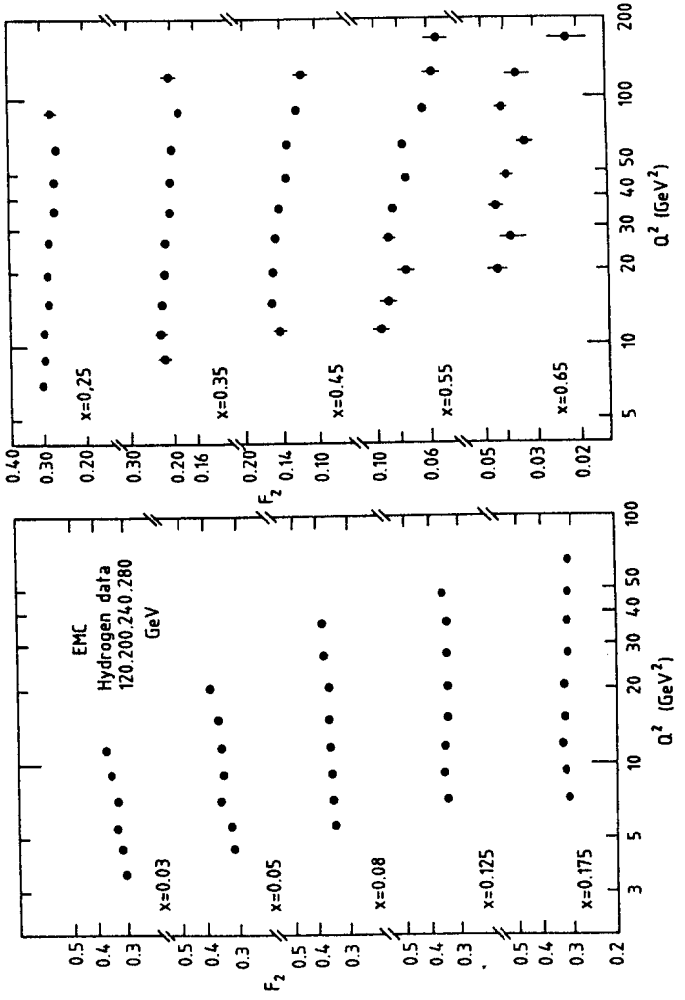

Fig. 33 The structure function $F_2^{\mu p}(x,Q^2)$ from the EMC experiment is shown as a function of Q^2 for different regions of x. (Ref. 30.)

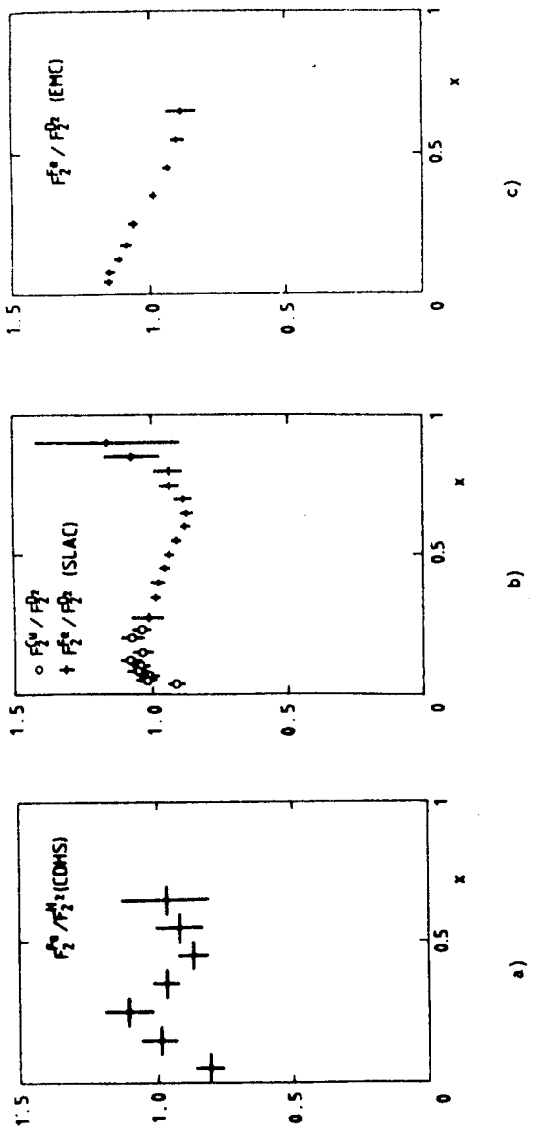

Fig. 34 EMC effect as observed in muon scattering (EMC, Ref. 32), electron scattering (SLAC, Ref. 33) and neutrino scattering (CDHS, Ref. 34).

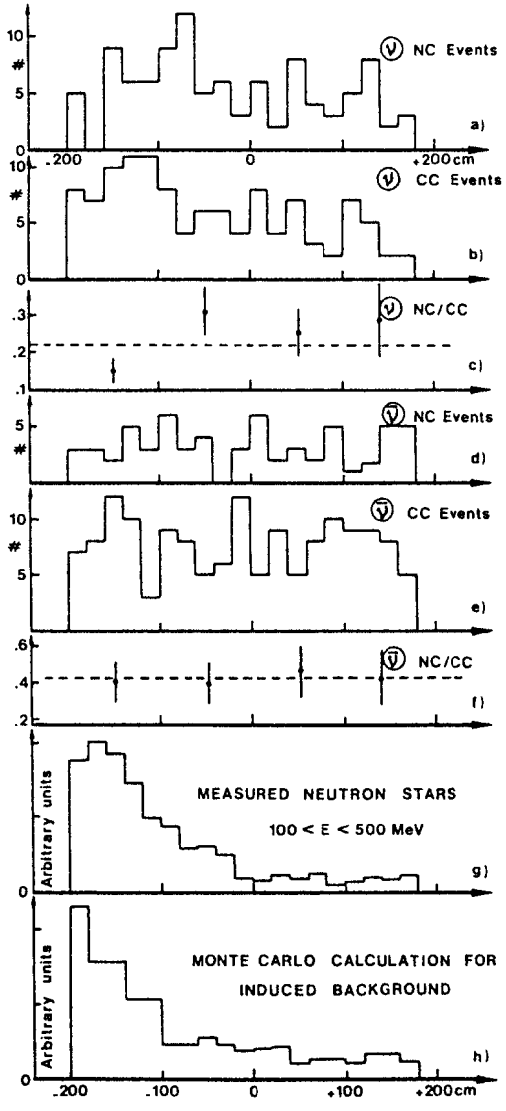

Fig. 35 Distribution of muonless events in Gargamelle along the beam direction. (Ref. 37.)

found. This discovery is of the utmost importance in the recent evolution of particle physics. It was soon confirmed in the electronic detector experiments at Fermilab,[38] where the experimental conditions were much more favorable, partly because of the higher rates and partly because of the higher energy, which permits a cleaner rejection of muon events.

5.2 Inclusive neutrino scattering and $\sin^2\theta_W$

Neutrino interactions provide several possibilities for the measurement of the Weinberg angle, as well as critical checks of the theory; the most precise of these at present come from the measurement of the neutral-to-charged-current total cross-section ratios:

$$\frac{\sigma(\nu \to \nu)}{\sigma(\nu \to \mu^-)} = R_\nu = \left[\frac{1}{2} - \sin^2\theta_W + \frac{5}{9}\sin^4\theta_W(1+r)\right]$$

and

$$\frac{\sigma(\bar{\nu} \to \bar{\nu})}{\sigma(\bar{\nu} \to \mu^+)} = R_{\bar{\nu}} = \left[\frac{1}{2} - \sin^2\theta_W + \frac{5}{9}\sin^4\theta_W\left(1+\frac{1}{r}\right)\right] ,$$

where

$$r = \frac{\sigma(\bar{\nu} \to \mu^+)}{\sigma(\nu \to \mu^-)} = 0.48 \pm 0.02^{21} .$$

The first precise measurement, in which the presently accepted value of $\sin^2\theta_W$ was found, is due to CDHS.[39] The neutral-current events are separated from the charged-current events on the basis of the short lengths of the event in the detector, since the charged-current events, with their penetrating muons, are in general long (see Fig. 36). To obtain the needed ratios, substantial corrections for short muons, electron-neutrino events, etc., have to be applied, but these can be determined with some precision. A compilation[40] of the most recent results is shown in Fig. 37. As can be seen from the figure, the determination is essentially due to R_ν; the $R_{\bar{\nu}}$ measurement serves as an important check on the theory and the method. The combined result, after electroweak radiative corrections, is:

$$\sin^2\theta_W = 0.223 \pm 0.007\ (\text{exp.}) \pm 0.006\ (\text{theor.}) .$$

The theoretical error is an estimate of uncertainties due to the strong interaction complications.

5.3 Inclusive polarized electron scattering and $\sin^2\theta_W$

In 1978, at SLAC, a new parity-violating effect in the scattering of longitudinally polarized electrons on deuterium[41] was observed. This is the asymmetry

$$A = \frac{\sigma_R - \sigma_L}{\sigma_R + \sigma_L}$$

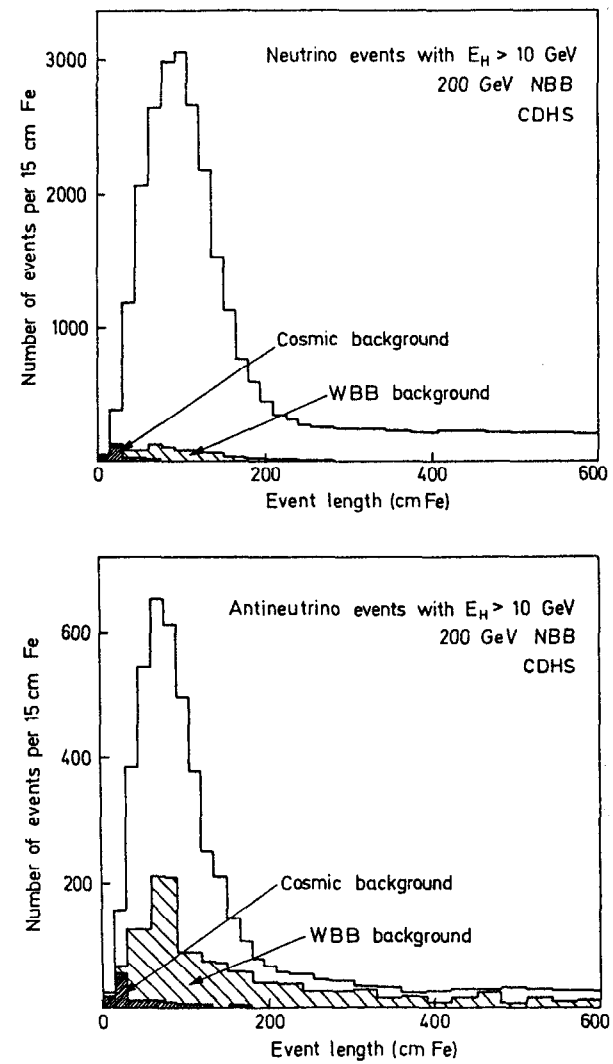

Fig. 36 Event length distribution of neutrino events in the CDHS detector. The peak at small event lengths is due to neutral-current events.

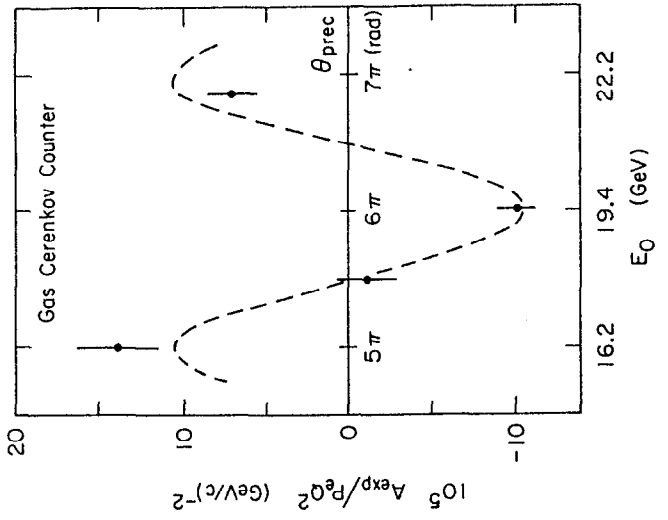

Fig. 38 Asymmetry in the scattering of longitudinally polarized electrons on deuterium as a function of the beam energy. (Ref. 41.)

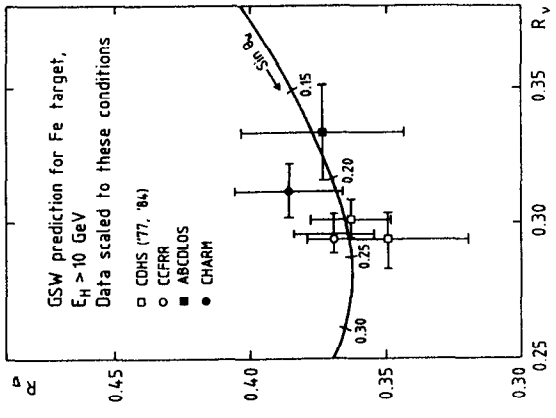

Fig. 37 Compilation of recent inclusive neutrino and anti-neutrino measurements to determine the weak mixing angle.

due to the interference of the electromagnetic and the neutral weak currents:

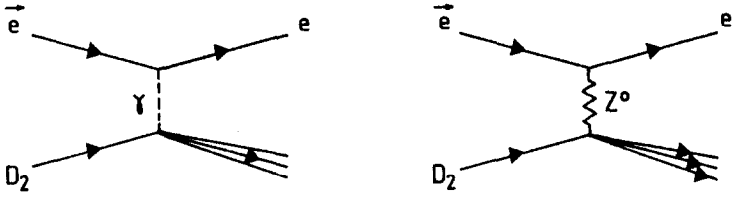

In the standard theory

$$A(y) = \frac{GQ^2}{\sqrt{2}\pi\alpha} \cdot \frac{9}{20}\left[\left(1 - \frac{20}{9}\sin^2\theta_W\right) + (1 - 4\sin^2\theta_W)\cdot\frac{1-(1-y)^2}{1+(1-y)^2}\right].$$

One of the several delightful checks on the experiment is reproduced in Fig. 38. It shows the behavior of the asymmetry with respect to beam energy. The helicity of the beam rotates with beam energy due to the $g-2$ precession in the beam transport, and the asymmetry follows this spin rotation, as can be seen in Fig. 38. The asymmetry measurements were later extended[42] to cover different regions in y, to provide an additional check on the theory (Fig. 39). The result quoted by the authors, $\sin^2\theta_W = 0.224 \pm 0.02$ has been corrected for electroweak radiative effects to compare with the neutrino results and also with the measured W^* and Z^0 masses:

Experiment	$\sin^2\theta_W$
Neutral-to-charged-current ratio in neutrino interactions	$0.223 \pm 0.007 \pm 0.006$ [a]
Asymmetry in $\vec{e}d$ scattering	$0.215 \pm 0.015 \pm 0.005$
W and Z masses from UA1 and UA2 $p\bar{p}$ experiments	
$M_W = 82.1 \pm 1.7$ GeV	
$M_Z = 93.0 \pm 1.7$ GeV	0.220 ± 0.009

a) The first error is the experimental error and the second error is due to uncertainties in the theoretical interpretation.

Here we have three very different experimental results, all three precisely measured, all understood in terms of a single parameter. This is very strong support for the 'standard' theory.

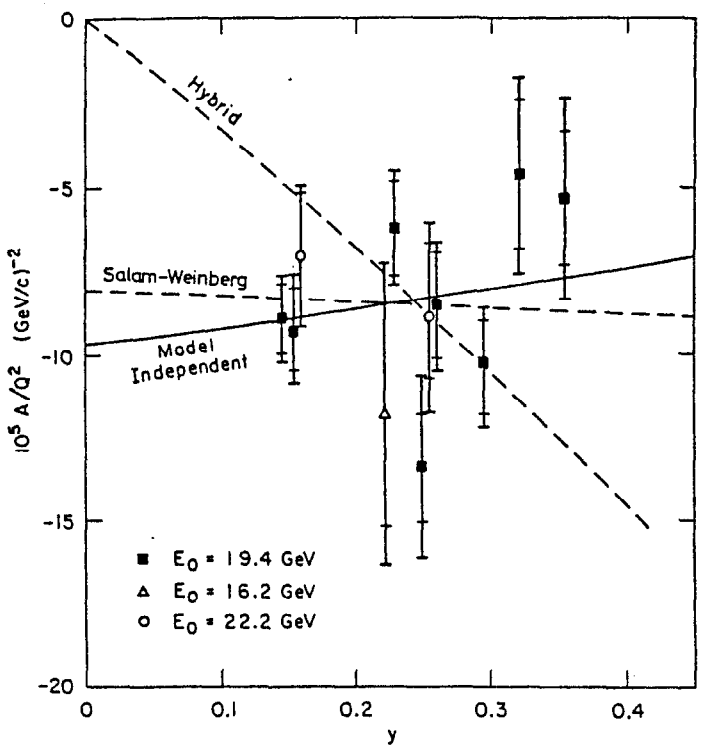

Fig. 39 Asymmetry as a function of y. (Ref. 42.)

REFERENCES

1. See, for example, E.E. Chambers an d R. Hofstadter, Phys. Rev. **103**, 1454 (1956).
2. G. Danby, J.M. Gaillard, L.M. Lederman, N. Mistry, M. Schwartz and J. Steinberger, Phys. Rev. Lett. **9**, 36 (1962).
3. W.K.H. Panofsky, C.M. Newton and G.B. Yodh, Phys. Rev. **98**, 751 (1955).
4. W.K.H. Panofsky, W.M. Woodward and G.B. Yodh, Phys. Rev. **102**, 1392 (1956).
5. G.B. Yodh and W.K.H. Panofsky, Phys. Rev. **105**, 731 (1957).
6. W.K.H. Panofsky and E.A. Allton, Phys. Rev. **110**, 1155 (1958).
7. A.A. Cone, K.W. Chen, J.R. Dunning, C. Hartwig, F.N. Ramsey, J.R. Walker and Richard Wilson, Phys. Rev. Lett. **14**, 326 (1965).
8. W. Albrecht, F.W. Brasse, H. Dorner, W. Flanger, K. Frank, J. Gayler, H. Hultschig and J. May, Phys. Lett. **25B**, 225 (1968).
9. The report, presented by J.I. Friedman at the 14th Int. Conf. on High Energy Physics, Vienna, 1968, is not published in the Conference Proceedings. It was, however, produced as a SLAC preprint.
10. J.D. Bjorken, Proc. Int. School of Physics 'Enrico Fermi', Course XLI: Selected Topics in Particle Physics (ed. J. Steinberger) (Academic Press, New York, 1968), p. 55.
    See also J. Bjorken, Phys. Rev. **179**, 1547 (1969).
11. W.K.H. Panofsky, Proc. 14th Int. Conf. on High Energy Physics, Vienna, 1968 (CERN, Geneva, 1968), p. 23.
12. R. Taylor, letter written in 1980. I am indebted to Professor Taylor for a copy of this letter.
13. Letter of J. Bjorken to the author, 1984.
14. E.D. Bloom et al., Phys. Rev. Lett. **23**, 930 (1969);
    M.L. Breidenbach et al., Phys. Rev. Lett. **23**, 935 (1969).
15. E.D. Bloom et al., SLAC-PUB 796, Sept. 1970, presented at the 15th Int. Conf. on High Energy Physics, Kiev, 1970.
16. M.D. Mestayer, Thesis, SLAC Report No. 214, August 1978.
17. R.E. Taylor, Proc. EPS Int. Conf. on High Energy Physics, Palermo, 1975 (Editrice Compositori, Bologna, 1976), p. 377.
18. A. Bodek et al., Phys. Rev. **D20**, 1471 (1979).
19. T. Eichten et al. Phys. Lett. **46B**, 274 (1973).
20. H. Deden et al., Nucl. Phys. **B85**, 269 (1975).
21. J.G.H. de Groot et al., Z. Phys. **C1**, 143 (1979).
22. H. Abramowicz et al., Z. Phys. **C13**, 199 (1982).
23. M.V. Purohit, Ph.D. Thesis, Columbia University Nevis Report No. 1298 (1983).
24. H. Abramowicz et al., Phys. Lett. **107B**, 141 (1981).
25. See, for example, the review of H.D. Politzer, Phys. Rep. **14C**, 129 (1974).
26. G. Altarelli and G. Parisi, Nucl. Phys. **B126**, 298 (1979).
27. H. Abramowicz et al., Z. Phys. **C12**, 289 (1982).
28. C. Chang et al., Phys. Rev. Lett. **35**, 901 (1975).

29. J.J. Aubert et al., Phys. Lett. **105B**, 315 (1981).
30. Presented by S.J. Wimpenny, EMC Collaboration, at the Int. Conf. on High Energy Physics, Brighton, July 1983.
31. J.J. Aubert et al., Phys. Lett. **114B**, 291 (1982).
32. J.J. Aubert et al., Phys. Lett. **123B**, 275 (1983).
33. A. Bodek et al., Phys. Rev. Lett. **50**, 1431 (1983).
34. H. Abramowicz et al., Z. Phys. **C25**, 29 (1984).
35. S.L. Glashow, Nucl. Phys. **22**, 579 (1961).
S. Weinberg, Phys. Rev. Lett. **19**, 1264 (1967).
G. 't Hooft, Nucl. Phys. **B35**, 167 (1971).
36. S.L. Glashow, J. Iliopoulos and L. Maiani, Phys. Rev. **D2**, 1285 (1970).
37. F. J. Hasert et al., Phys. Lett. **46B**, 138 (1973).
38. A. Benvenuti et al., Phys. Rev. Lett. **32**, 800 (1974).
B.C. Barish et al., Phys. Rev. Lett. **34**, 538 (1975).
39. M. Holder et al., Phys. Lett. **71B**, 222 (1977).
40. C. Geweniger, presented at the 11th Int. Conf. on Neutrino Physics and Astrophysics, Dortmund, 1984.
41. C.Y. Prescott et al., Phys. Lett. **77B**, 347 (1978).
42. C.Y. Prescott et al., Phys. Lett. **84B**, 524 (1979).